Published in final edited form as:
J Phys Chem Lett. 2011 June 30; 2011(2): 1771–1776. doi:10.1021/jz2007676.

Theory and Simulation of the Environmental Effects on FMO Electronic Transitions

Carsten Olbrich[†], **Johan Strümpfer**[‡], **Klaus Schulten**[‡,¶], and **Ulrich Kleinekathöfer**[*,†]

[†]School of Engineering and Science, Jacobs University Bremen, Campus Ring 1, 28759 Bremen, Germany

[‡]Center for Biophysics and Computational Biology and Beckman Institute, University of Illinois at Urbana-Champaign, Urbana, Illinois 61801, USA

[¶]Department of Physics, University of Illinois at Urbana-Champaign, Urbana, Illinois 61801, USA

Abstract

Long-lived quantum coherence has been experimentally observed in the Fenna-Matthews-Olson (FMO) light-harvesting complex. It is much debated which role thermal effects play and if the observed low-temperature behavior arises also at physiological temperature. To contribute to this debate we use molecular dynamics simulations to study the coupling between the protein environment and the vertical excitation energies of individual bacteriochlorophyll molecules in the FMO complex of the green sulphur bacterium *Chlorobaculum tepidum*. The so-called spectral densities, which account for the environmental influence on the excited state dynamics, are determined from temporal autocorrelation functions of the energy gaps between ground and first excited states of the individual pigments. Although the overall shape of the spectral density is found to be rather similar for all pigments, variations in their magnitude can be seen. Differences between the spectral densities for the pigments of the FMO monomer and FMO trimer are also presented.

Keywords

Fenna-Matthews-Olson complex; spectral density; environmental effects; mixed quantum-classical simulations; exciton dynamics

Many plants and bacteria acquire their energy from sunlight through photosynthesis. Light harvesting is arguably thus the most important process of energy acquisition on earth. Green sulfur bacteria and some other phototrophs use large vesicles of pigments, called chlorosomes, as their main antenna for capturing photons. The resulting excitation energy is then transferred across the so-called Fenna-Matthews-Olson (FMO) complex to the reaction center where it is used to establish a charge gradient across the membrane.[1] The crystal structure of the FMO complex from the bacterium *Prosthecochloris aestuarii* was first resolved in 1979.[2] An improved structure at atomic resolution of 1.9 Å was reported later[3] as was a high-resolution structure for *Chlorobaculum tepidum*.[4] The FMO complex forms a homo-trimer under physiological conditions, with each monomer containing eight bacteriochlorophyll-a (BChl a) molecules (see Figure 1).

[*]To whom correspondence should be addressed u.kleinekathoefer@jacobs-university.de.

Supporting Information Available

Tables listing the parameters of the autocorrelation function fits and results for the monomer simulations. This material is available free of charge via the Internet at http://pubs.acs.org/.

Long-lived coherence effects in time-resolved optical two-dimensional spectra[5–7] spurred a tremendous interest in the FMO complex.[8] In similar experiments, long-lasting coherence beating signals have also been observed for a photosynthetic complex of marine algae at ambient temperature[9] as well as in conjugated polymers.[10] The obvious and so far open question is how such effects can survive several hundred femtoseconds within a biological environment at low and physiological temperatures. In general one expects quantum effects to decay within tens of femtoseconds due to the thermal fluctuations inherent in a complex and disordered biological environment. As a result of stated observations, several theoretical studies have been performed to explore this long-lived coherent beating phenomenon (see, e.g., Refs. 11–19). It was suggested that long-lived coherent beating arises from correlated fluctuations of the pigment molecules. In DNA, for example, the neighboring entities are close to each other to experience partially the same electrostatic potential of the surrounding, leading to spatial site correlations that have a drastic effect on electronic transport properties.[20] We have recently shown, however, using classical molecular dynamics (MD) simulations and semiemperical electronic structure calculations, that correlations between pigment excitation energy fluctuations most likely do not exist in the FMO complex.[21,22] Interference of different quantum pathways have also been proposed as the origin of the long-lived coherences.[18,23]

The spectral density is the key quantity, for all the theoretical investigations using a density matrix approach, to describe the system-environment interaction and, hence, thermal effects.[24,25] For the FMO complex, experimental investigations on the electron-vibrational coupling have been reported earlier.[26] The spectral density for light-harvesting complex 2 (LH2) has previously been extracted from a combination of MD and electronic structure calculations.[27–30] Recently we have used the same approach, i.e., MD and quantum chemistry calculations on the ZINDO/S level (Zerner Intermediate Neglect of Differential Orbital method with parameters for spectroscopic properties) to constructed a time-dependent Hamiltonian for the FMO complex.[21,22] That Hamiltonian was subsequently employed to determine room temperature exciton population dynamics, linear absorption and 2D spectra by using it in an ensemble-averaged wave packet formalism, termed NISE (numerical integration of the Schrödinger equation).[31,32] The drawback of NISE is its implicit assumption of an infinite temperature and that it therefore does not yield the correct thermal equilibrium at finite temperatures. In the present report the same trajectories of the energy gap fluctuations between the BChl ground and first excited states, i.e. the BChl Q_y state, are used to extract the spectral densities of the individual FMO BChls. FMO spectral densities based on the analysis of experimental results have also been proposed by Adolphs and Renger,[33] by Cho and coworkers[34] as well as by Ishizaki and Fleming.[11] Very recently another computational study has been reported as well.[35]

For the details of the MD and ZINDO/S calculations we refer the reader to Refs. 21 and 22. The MD is a ground state MD which includes approximations due to the underlying force field. The energy gap fluctuations for BChls of both the FMO trimer and the FMO monomer have been determined using the semi-empirical ZINDO/S method which was parametrized for the BChl molecules. For the trimer, for example, 24 energy gap calculations per snapshot have been performed for 40,000 snapshot amounting to almost a million ZINDO/S calculations. Though the ZINDO/S method has its limitations, it has been shown to treat environmental effects in chromophores more accurately than, e.g., density functional-based approaches.[36] Since FMO forms a trimer under physiological conditions, the trimer data are described below while the corresponding monomer data are presented in the supporting information.

The first step in the process of obtaining spectral densities is calculating the autocorrelation function of the energy gap between ground and first excited state. In principle the

autocorrelation functions are different for each pigment. In case of the trimer simulations we average over the equivalent pigments in the three monomers. The autocorrelation function is determined using the energy gaps $\Delta E_{j,l}(t_i)$ at time steps t_i for BChl j in monomer l. Including an average over M equivalent BChls, the autocorrelation function $C_j(t_i)$ is given by[27]

$$C_j(t_i)=\frac{1}{M}\sum_{l=1}^{M}\left[\frac{1}{N-i}\sum_{k=1}^{N-i}\Delta E_{j,l}(t_i+t_k)\Delta E_{j,l}(t_k)\right]. \quad (1)$$

For the monomer simulations there are no equivalent BChls and M therefore equals one while for the trimer its value is three. The fastest oscillations in the site energies have periods of around 20 fs and therefore we choose a time step of 5 fs between the individual snapshots of the MD and ZINDO/S calculations. For the monomer simulations the time series contains 60,000 and for the trimer simulations 40,000 points. The correlation functions quickly decay, within the first 100–200 fs, and vanish within 1–2 ps. Therefore 4 ps-long windows were used to determine correlation functions of 2 ps length. Using a spacing of 1 ps, there are 296 and 196 4 ps-long windows along the trajectories for the trimer and monomer, respectively. The correlation functions were calculated for each window and then averaged. At long times their values should be zero by definition. Due to the averaging procedure the autocorrelation functions sometimes exhibit a small offset, which is discarded in the fitting procedure. The resulting correlation function for the trimer are shown in Figure 2 and for the monomer in Fig. S1. The correlation functions for BChl 1 to 6 behave to some extend rather similarly with larger deviations for pigments 7 and 8. To keep the number of different functional forms simple, we decided to only use one averaged spectral density for BChls 1 to 6 but separate ones for BChl 7 and 8. The respective spectral densities for the individual BChls can be found in the supporting information.

In case of LH2[29] we fitted the correlation functions to an analytical form, i.e., a combination of exponentials and damped oscillations

$$C_j(t)\approx\sum_{i=1}^{N_e}\eta_{j,i}e^{-\gamma_{j,i}t}+\sum_{i=1}^{N_o}\tilde{\eta}_{j,i}\cos(\tilde{\omega}_{j,i}t)e^{-\tilde{\gamma}_{j,i}t}. \quad (2)$$

Below two different fitting functions are used. The first one, called Fit 1, used two exponentials ($N_e = 2$) and 13 damped oscillations ($N_o = 13$) while a simplified version, called Fit 2, uses two exponentials only ($N_e = 2$, $N_o = 0$). Both fits are shown together with the original correlation functions in Figure 2. The parameters for the simplified fitting form are given in Table 1 while the ones for the more elaborate fits are given in Table S1. The corresponding data for the monomer are listed in Tables S2 and S3. Looking at the double-exponential fit, the fast initial decay has a decay time $\tau_i = 1/\gamma_i$ of about 4–5 fs for all BChls while the slower decay time is 140 fs for pigments 1–6 and 8 while it is 230 fs for BChl 7. Beyond these two exponential decays the correlation function shows strong oscillations with oscillation periods around 20 fs. These oscillations can be attributed to vibrational motions including C=C and C=O double bonds.[27,29,37–39]

The spectral density $J(\omega)$ describes the frequency-dependent coupling between the excitonic sub-system and the thermal environment. Denoting the inverse temperature by $\beta = 1/(k_B T)$ the spectral density $J_j(\omega)$ of BChl j is given by[27,40,41]

$$J_j(\omega)=\frac{2}{\pi\hbar}\tanh(\beta\hbar\omega/2)\int_0^\infty \mathrm{d}t\, C_j(t)\cos(\omega t), \quad (3)$$

which is the key relation for combining the results from the MD and quantum chemistry studies with dissipative exciton dynamics. We note that the spectral density in the Caldeira-Leggett model $J_{CL,j}(\omega)$ is connected to the present form by $J_{CL,j}(\omega)=\frac{\pi}{\hbar}J_j(\omega)$. The thermal correction factor in Eq. (3) fulfills two functions: it ensures the validity of the detailed balance relation and at the same time (approximately) removes the temperature dependence from the spectral density. The fluctuations in the MD simulations are of course temperature dependent but the spectral density is, assuming a harmonic bath, a temperature-independent quantity.

Using the analytic expression for $C(t)$, Eq. (2), the spectral density is given by

$$J_j(\omega)=\frac{2}{\pi\hbar}\tanh(\beta\hbar\omega/2)\left[\sum_{i=1,2}^{N_e}\frac{\eta_{j,i}\gamma_{j,i}}{\gamma_{j,i}^2+\omega^2}+\sum_{i=1,10}^{N_o}\frac{\tilde{\eta}_{j,i}\tilde{\gamma}_{j,i}}{2(\tilde{\gamma}_{j,i}^2+(\omega-\tilde{\omega}_{j,i})^2)}\right]. \quad (4)$$

In this expression we have neglected terms similar to the last term in Eq. (4) but with $(\omega + \tilde{\omega}_i)^2$ instead of $(\omega - \tilde{\omega}_i)^2$ in the denominator. Including these terms leads to negligible changes in the values of the spectral density. Furthermore, we note that in most applications concerning electronic relaxation one is only interested in the low energy range and many of the high-energy features of the spectral density might be rather unimportant for these applications.

The resulting spectral densities are displayed in Figure 3. Shown in this figure is the averaged spectral density for BChl 1 to 6 and the distinctly larger spectral densities for BChl 7 and 8. The forms of all the spectral densities are very similar, only their amplitudes differ considerably. The bi-exponential Fit 2 leads to a rather featureless electron-environment coupling. The exponential with the long time constant leads to a sharp rise of the spectral density at small frequencies. In the low-energy regime the difference between spectral densities resulting from Fit 1 and Fit 2 is minor. For many purposes, the simpler spectral density might thus be sufficient. It is no surprise that BChl 8 shows a larger spectral densities since it is weakly bound to the complex. In the monomer simulations, BChl 8 even left the complex. BChl 7 on the other hand, seems to have a more fluctuating environment than the other BChls. A detailed analysis including the usage of the electrostatic potential as previously done for DNA in water[42] is currently underway. Shown in Figure 4 is the comparison between spectral densities calculated using the ZINDO/S with and without taking the charges external to each BChl into account. It becomes clear that the low energy part of the spectral densities is mainly due to the fluctuations of the environment. Interestingly, basically all peaks in the spectral densities already appear without taking into account the external charges and are therefore internal modes. The fluctuation strengths of these internal modes are influenced by the fluctuating environment.

In a previous study[29] we analyzed the spectral densities for LH2 of the purple bacterium *Rhodospirillum molischianum*, which were determined using the same approach as employed in the present investigation. The LH2 system consists of two bacteriochlorophyll systems, the B800 and the B850 rings. The BChl in these two rings experience different environments leading to two different spectral densities.[29] In Figure 5 the spectral densities for the BChls in the B800 and B850 rings are compared to those from the FMO complex. Again there is a quite large agreement concerning the functional form but not the amplitude of the different spectral densities. Since the BChl molecules are in different protein environments, the similarities of their spectral densities most likely result from their internal vibrations. For example, it is well known that BChl molecules have vibrational modes in the region of 1600 cm^{-1} which are strongly present in Figure 5. The rather featureless

background of the spectral densities, especially in the low energy region, differs between environments and seems to be mainly due to electrostatic interactions with vibrational modes outside of the individual pigment.

After comparing to spectral densities obtained using the same approach for a different system, we compare, as shown in Figure 6, the present results for the FMO complex with previous approximations for the spectral density, all of them assuming equal properties for all BChls. Adolphs and Renger estimated the electron-environment coupling based on the fluorescence line narrowing spectrum.[33] This spectral density has a maximum at around 0.02 eV and decays exponentially at larger energies. The Fleming group has proposed two other spectral densities,[11,34] which do not differ greatly from that of Adolphs and Renger, but decay even faster at energies above 0.01 eV. The amplitudes of these spectral densities are considerably smaller than the ones determined in the current work. Recently, Nalbach *et al.*[19] employed the spectral density of Adolphs and Renger with the addition of a single vibrational mode. Interestingly, the spectral density with this additional broad mode only leads to small differences in the exciton dynamics.[19]

At energies below 0.01 eV the present system-bath interaction for BChl 1 to 6 is about a factor 2–3 larger and extends to higher energies than those reported previously.[11,19,33,34] The present system-bath interaction is, however, in agreement with that of chlorophyll a molecules, which have been proposed in the form of Huang-Rhys factors that also extend to energies of about 0.2 eV.[43,44] Furthermore, it is not surprising that the system-bath interaction is non-vanishing for energies around 0.2 eV since there are several C=O, C=C bonds in chlorophyll and BChl molecules which vibrate with frequencies in this region. In the present approach internal BChl modes as well as external environmental effects that lead to fluctuations in the energy gap between ground and first excited state are included. The internal modes of BChl based on density functional and force field calculations appear in the same energy range and with a qualitatively similar distribution as shown in the high-energy region of the present spectral density.[39]

Based on the same MD and electronic energy gap calculations as employed here, we previously presented data on the linear absorption and two-dimensional spectra of FMO at room temperature. [22] Disorder due to large-scale structural changes were, however, not included in those calculations. These changes are on time scales much longer than accessible by standard MD simulations and are usually modelled as static disorder. Therefore spectral features of the linear and 2D spectra showed narrower widths than are observed experimentally. This discrepancy suggests that the time-dependent Hamiltonian, used as the basis for the present results, does not contain to a sufficient degree large amplitude fluctuations. The ensemble-averaged wave packet dynamics used in Ref. 22 has the drawback that it includes an implicit high-temperature limit, i.e., it leads to incorrect site populations in the long-time limit; some density matrix approaches which could employ the present spectral density usually do not suffer from this drawback. For room temperature systems, however, we do not expect a significant difference for the linear absorption and two-dimensional spectra and therefore refrain from repeating the calculations using these approaches. Nevertheless, the agreement between the spectra calculated using wave packet dynamics and experimental spectra indicate that the amplitude of our spectral densities, though larger than previous estimates, are in accordance with experiments.

The present results make it possible to computationally investigate the effects of the experimentally observed long-lived coherence in FMO.[5–7] The impetus to understand these underlying effects has steered many investigations (see, e.g., Refs. 12–19,45) which sometimes assumed rather crude approximations for the system-bath interaction. Other simulations were based on spectral densities by Adolphs and Renger[33] or the Fleming

group.[11,34] All these spectral densities were derived based upon specific experimental information which might not cover the whole energy range as discussed above. The present spectral densities based on atomistic simulations partially differ for the individual BChls, cover a large frequency range and make further studies of electronic properties of the FMO complex possible.

Supplementary Material

Refer to Web version on PubMed Central for supplementary material.

Acknowledgments

This work has been supported by grant KL 1299/3-1 of the Deutsche Forschungsgemeinschaft (DFG), the National Institute of Health (NIH) and the National Science Foundation (NSF). Funding for J.S. and K.S. was provided by NSF grants MCB-0744057, PHY0822613 and NIH grant P41- RR05969.

References

1. Wen J, Zhang H, Gross ML, Blankenship RE. Membrane Orientation of the FMO Antenna Protein from Chlorobaculum tepidum as determined by Mass Spectrometry-based Footprinting. Proc. Natl. Acad. Sci. USA. 2009; 106:6134–6139. [PubMed: 19339500]
2. Matthews BW, Fenna RE, Bolognesi MC, Schmid MF, Olson JM. Structure of a Bacteriochlorophyll a-Protein from the Green Photosynthetic Bacterium. Prosthecochloris aestuarii. J. Mol. Biol. 1979; 131:259–265.
3. Tronrud DE, Schmid MF, Matthews BW. Structure and X-ray Amino Acid Sequence of a Bacteriochlorophyll a Protein from *Prosthecochloris aestuarii* Refined at 1.9 Å Resolution. J. Mol. Biol. 1986; 188:443–444. [PubMed: 3735428]
4. Tronrud DE, Wen J, Gay L, Blankenship RE. The Structural Basis for the Difference in Absorbance Spectra for the FMO Antenna Protein from Various Green Sulfur Bacteria. Photosynth. Res. 2009; 100:79–87. [PubMed: 19437128]
5. Brixner T, Stenger J, Vaswani HM, Cho M, Blankenship RE, Fleming GR. Two-Dimensional Spectroscopy of Electronic Couplings in Photosynthesis. Nature. 2005; 434:625–628. [PubMed: 15800619]
6. Engel GS, Calhoun TR, Read EL, Ahn TK, Mancal T, Cheng YC, Blankenship RE, Fleming GR. Evidence for Wavelike Energy Transfer through Quantum Coherence in Photosynthetic Systems. Nature. 2007; 446:782–786. [PubMed: 17429397]
7. Panitchayangkoon G, Hayes D, Fransted KA, Caram JR, Harel E, Wen J, Blankenship RE, Engel GS. Long-Lived Quantum Coherence in Photosynthetic Complexes at Physiological Temperature. Proc. Natl. Acad. Sci. USA. 2010; 107:12766–12770. [PubMed: 20615985]
8. Scholes GD. Quantum-Coherent Electronic Energy Transfer: Did Nature Think of It First? J. Phys. Chem. Lett. 2010; 1:2–8.
9. Collini E, Wong CY, Wilk KE, Curmi PM, Brumer P, Scholes GD. Coherently Wired Light-Harvesting in Photosynthetic Marine Algae at Ambient Temperature. Nature. 2010; 463:644–647. [PubMed: 20130647]
10. Collini E, Scholes GD. Coherent Intrachain Energy Migration in a Conjugated Polymer at Room Temperature. Science. 2009; 323:369–373. [PubMed: 19150843]
11. Ishizaki A, Fleming GR. Theoretical Examination of Quantum Coherence in a Photosynthetic System at Physiological Temperature. Proc. Natl. Acad. Sci. USA. 2009; 106:17255–17260. [PubMed: 19815512]
12. Caruso F, Chin AW, Datta A, Huelga SF, Plenio MB. Highly Efficient Energy Excitation Transfer in Light-Harvesting Complexes: The Fundamental Role of Noise-Assisted Transport. J. Chem. Phys. 2009; 131:105106.
13. Rebentrost P, Mohseni M, Aspuru-Guzik A. Role of Quantum Coherence and Environmental Fluctuations in Chromophoric Energy Transport. J. Phys. Chem. B. 2009; 113:9942–9947. [PubMed: 19603843]

14. Nazir A. Correlation-Dependent Coherent to Incoherent Transitions in Resonant Energy Transfer Dynamics. Phys. Rev. Lett. 2009; 103:146404. [PubMed: 19905588]
15. Fassioli F, Nazir A, Olaya-Castro A. Quantum State Tuning of Energy Transfer in a Correlated Environment. J. Phys. Chem. Lett. 2010; 1:2139–2143.
16. Nalbach P, Eckel J, Thorwart M. Quantum Coherent Biomolecular Energy Transfer with Spatially Correlated Fluctuations. New J. Phys. 2010; 12:065043.
17. Fleming GR, Huelga S, Plenio M. Focus on Quantum Effects and Noise in Biomolecules. New J. Phys. 2010; 12:065002.
18. Abramavicius D, Mukamel S. Quantum Oscillatory Exciton Migration in Photosynthetic Reaction Centers. J. Chem. Phys. 2010; 133:064510. [PubMed: 20707578]
19. Nalbach P, Braun D, Thorwart M. How "Quantum" is the Exciton Dynamics in the Fenna-Matthews-Olson Complex? 2011 arXiv:1104.2031v1.
20. Kubař T, Kleinekathöfer U, Elstner M. Solvent Fluctuations Drive the Hole Transfer in DNA: a Mixed Quantum-Classical Study. J. Phys. Chem. B. 2009; 113:13107–13117. [PubMed: 19725541]
21. Olbrich C, Strümpfer J, Schulten K, Kleinekathöfer U. Quest for Spatially Correlated Fluctuations in the FMO Light-Harvesting Complex. J. Phys. Chem. B. 2011; 115:758–764. [PubMed: 21142050]
22. Olbrich C, Jansen TLC, Liebers J, Aghtar M, Strümpfer J, Schulten K, Knoester J, Kleinekathöfer U. From Atomistic Modeling to Excitation Dynamics and Two-16 Dimensional Spectra of the FMO Light-Harvesting Complex. J. Phys. Chem. B. 2011 in press.
23. Dijkstra AG, Jansen TLC, Knoester J. Localization and Coherent Dynamics of Excitons in the Two-Dimensional Optical Spectrum of Molecular J-Aggregates. J. Chem. Phys. 2008; 128:164511. [PubMed: 18447463]
24. Heřman P, Kleinekathöfer U, Barvík I, Schreiber M. Exciton Scattering in Light-Harvesting Systems of Purple Bacteria. J. Lumin. 2001; 94&95:447–450.
25. Heřman P, Kleinekathöfer U, Barvík I, Schreiber M. Influence of Static and Dynamic Disorder on the Anisotropy of Emission in the Ring Antenna Subunits of Purple Bacteria Photosynthetic Systems. Chem. Phys. 2002; 275:1–13.
26. Wendling M, Pullerits T, Przyjalgowski MA, Vulto SIE, Aartsma TJ, Grondelle Rv, Amerongen Hv. Electron-Vibrational Coupling in the Fenna-Matthews-Olson Complex of Prosthecochloris aestuarii Determined by Temperature-Dependent Absorption and Fluorescence Line-Narrowing Measurement. J. Phys. Chem. B. 2000; 104:5825–5831.
27. Damjanović A, Kosztin I, Kleinekathöfer U, Schulten K. Excitons in a Photosynthetic Light-Harvesting System: A Combined Molecular Dynamics, Quantum Chemistry and Polaron Model Study. Phys. Rev. E. 2002; 65:031919.
28. Janosi L, Kosztin I, Damjanović A. Theoretical Prediction of Spectral and Optical Properties of Bacteriochlorophylls in Thermally Disordered LH2 Antenna Complexes. J. Chem. Phys. 2006; 125:014903. [PubMed: 16863329]
29. Olbrich C, Kleinekathöfer U. Time-dependent Atomistic View on the Electronic Relaxation in Light-Harvesting System II. J. Phys. Chem. B. 2010; 114:12427–12437. [PubMed: 20809619]
30. Olbrich C, Liebers J, Kleinekathöfer U. Modeling of Light-Harvesting in Purple Bacteria using a Time-Dependent Hamiltonian Approach. phys. stat. sol. (b). 2011; 248:393–398.
31. Jansen TLC, Knoester J. Nonadiabatic Effects in the Two-Dimensional Infrared Spectra of Peptides. J. Phys. Chem. B. 2006; 110:22910–22916. [PubMed: 17092043]
32. Jansen TLC, Knoester J. Waiting Time Dynamics in Two-Dimensional Infrared Spectroscopy. Acc. Chem. Res. 2009; 42:1405–1411. [PubMed: 19391619]
33. Adolphs J, Renger T. How Proteins Trigger Excitation Energy Transfer in the FMO Complex of Green Sulfur Bacteria. Biophys. J. 2006; 91:2778–2787. [PubMed: 16861264]
34. Cho M, Vaswani HM, Brixner T, Stenger J, Fleming GR. Exciton Analysis in 2D Electronic Spectroscopy. J. Phys. Chem. B. 2005; 109:10542–10556. [PubMed: 16852278]
35. Shim S, Rebentrost P, Valleau S, Aspuru-Guzik A. Microscopic Origin of the Long-Lived Quantum Coherences in the Fenna-Matthew-Olson Complex. arXiv:1104.2943v1.

36. Wanko M, Hoffmann M, Strodel P, Koslowski A, Thiel W, Neese F, Frauenheim T, Elstner M. Calculating Absorption Shifts for Retinal Proteins: Computational Challenges. J. Phys. Chem. B. 2005; 109:3606. [PubMed: 16851399]

37. Mercer IP, Gould IR, Klug DR. Optical Properties of Solvated Molecules Calculated by QMMM Methods: Chlorophyll a and Bacteriochlorophyll a. Faraday Discuss. 1997; 108:51–62.

38. Walker RC, Mercer IP, Gould IR, Klug DR. Comparison of Basis Set Effects and the Performance of ab initio and DFT Methods for Probing Equilibrium Fluctuations. J. Comput. Chem. 2007; 28:478–480. [PubMed: 17186476]

39. Ceccarelli M, Procacci P, Marchi M. An ab initio Force Field for the Cofactors of Bacterial Photosynthesis. J. Comput. Chem. 2003; 24:129–132. [PubMed: 12497594]

40. May, V.; Kühn, O. Charge and Energy Transfer in Molecular Systems. Berlin: Wiley-VCH; 2000.

41. Gutiérrez R, Caetano R, Woiczikowski PB, Kubař T, Elstner M, Cuniberti G. Structural Fluctuations and Quantum Transport Through DNA Molecular Wires: a Combined Molecular Dynamics and Model Hamiltonian Approach. New J. Phys. 2010; 12:023022.

42. Kubař T, Elstner M. What Governs the Charge Transfer in DNA? The Role of DNA Conformation and Environment. J. Phys. Chem. B. 2008; 112:8788–8788. [PubMed: 18582109]

43. Zucchelli G, Jennings RC, Garlaschi FM, Cinque G, Bassi R, Cremonesi O. The Calculated in vitro and in vivo Chlorophyll a Absorption Bandshape. Biophys. J. 2002; 82:378–390. [PubMed: 11751324]

44. Yang M, Damjanović A, Vaswani HM, Fleming GR. Energy Transfer in Photosystem I of Cyanobacteria Synechococcus elongatus: Model Study with Structure-Based Semi-Empirical Hamiltonian and Experimental Spectral Density. Biophys. J. 2003; 85:140–158. [PubMed: 12829471]

45. Strümpfer J, Schulten K. The Effect of Correlated Bath Fluctuations on Exciton Transfer. J. Chem. Phys. 2011; 134:095102. [PubMed: 21385000]

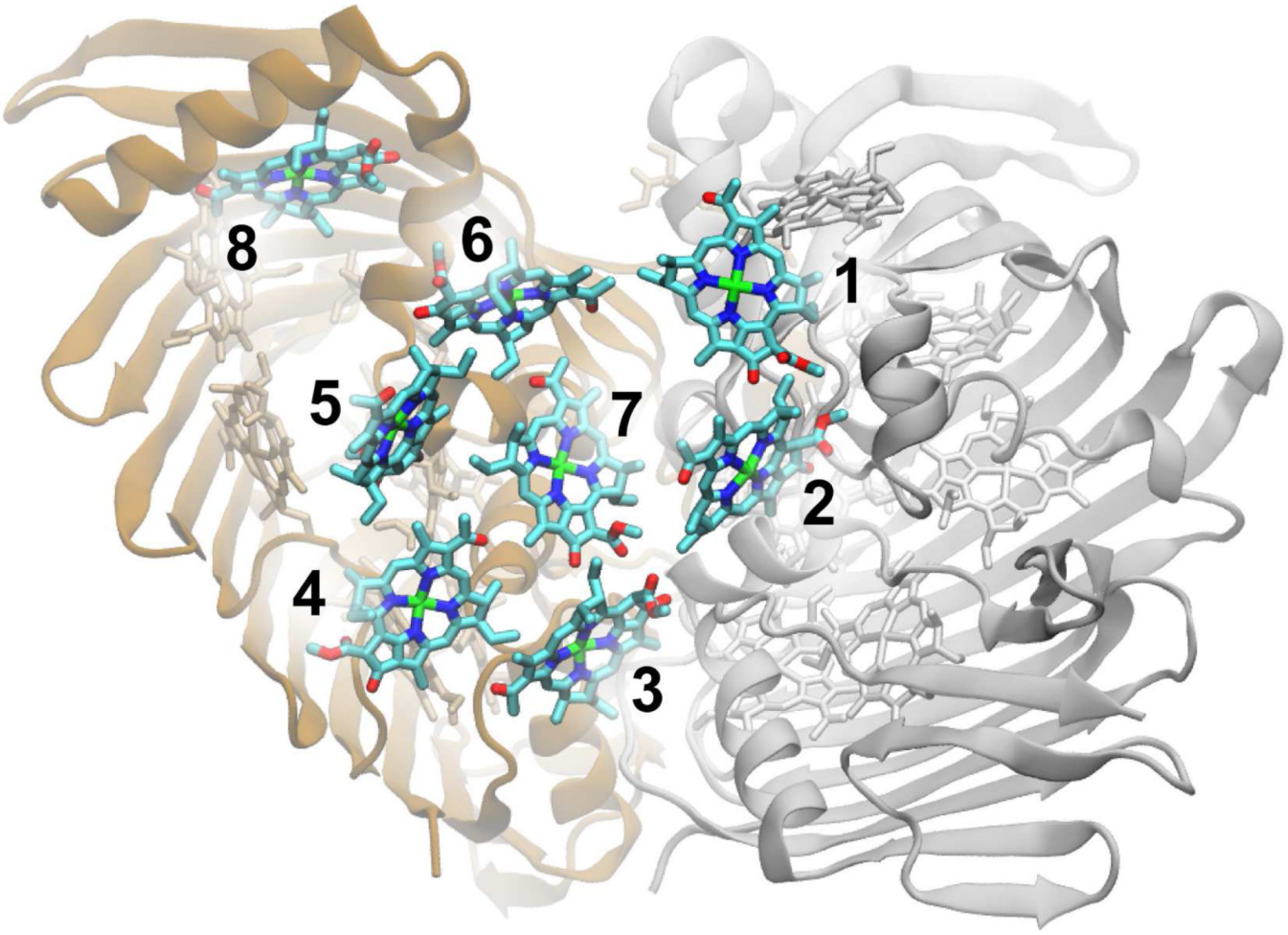

Figure 1.
The FMO trimer with the protein structure of two monomers shown in cartoon representation. Highlighted are the eight BChls of one monomer.

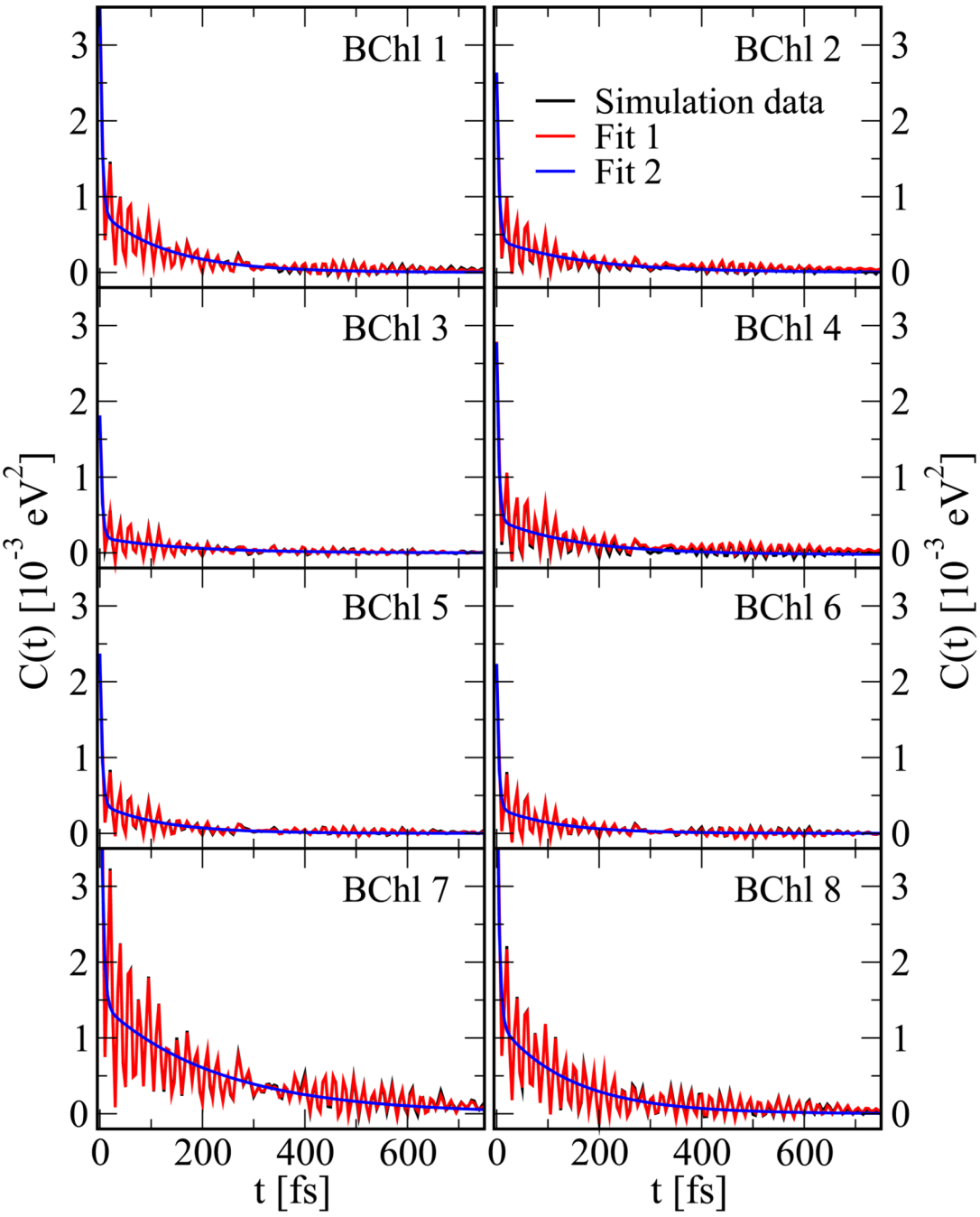

Figure 2.
Energy gap autocorrelation functions for the 8 different BChls of the FMO trimer. The simulation data have been averaged over the equivalent BChls in the three monomers. Shown are the data as obtained from the simulations (black), a series of exponential decays and damped oscillations (blue) as well as a double-exponential fit (red, see main text).

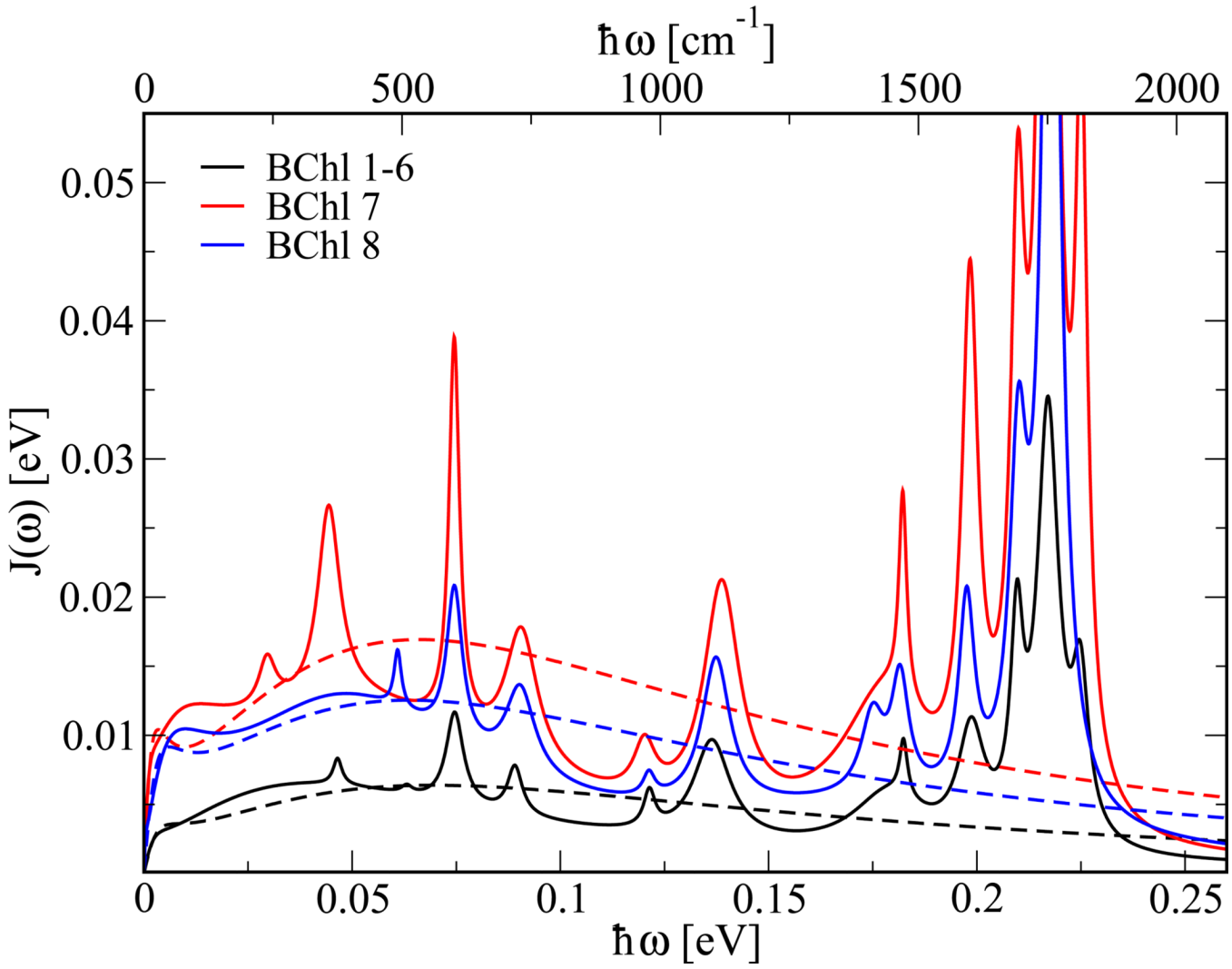

Figure 3.
Spectral densities of different BChls in the trimer. The spectral properties of BChl 1 to 6 are described by an averaged quantity. In addition to results based on Fit 1 (solid lines), approximate spectral densities based on Fit 2 to the correlations functions are shown (dotted lines).

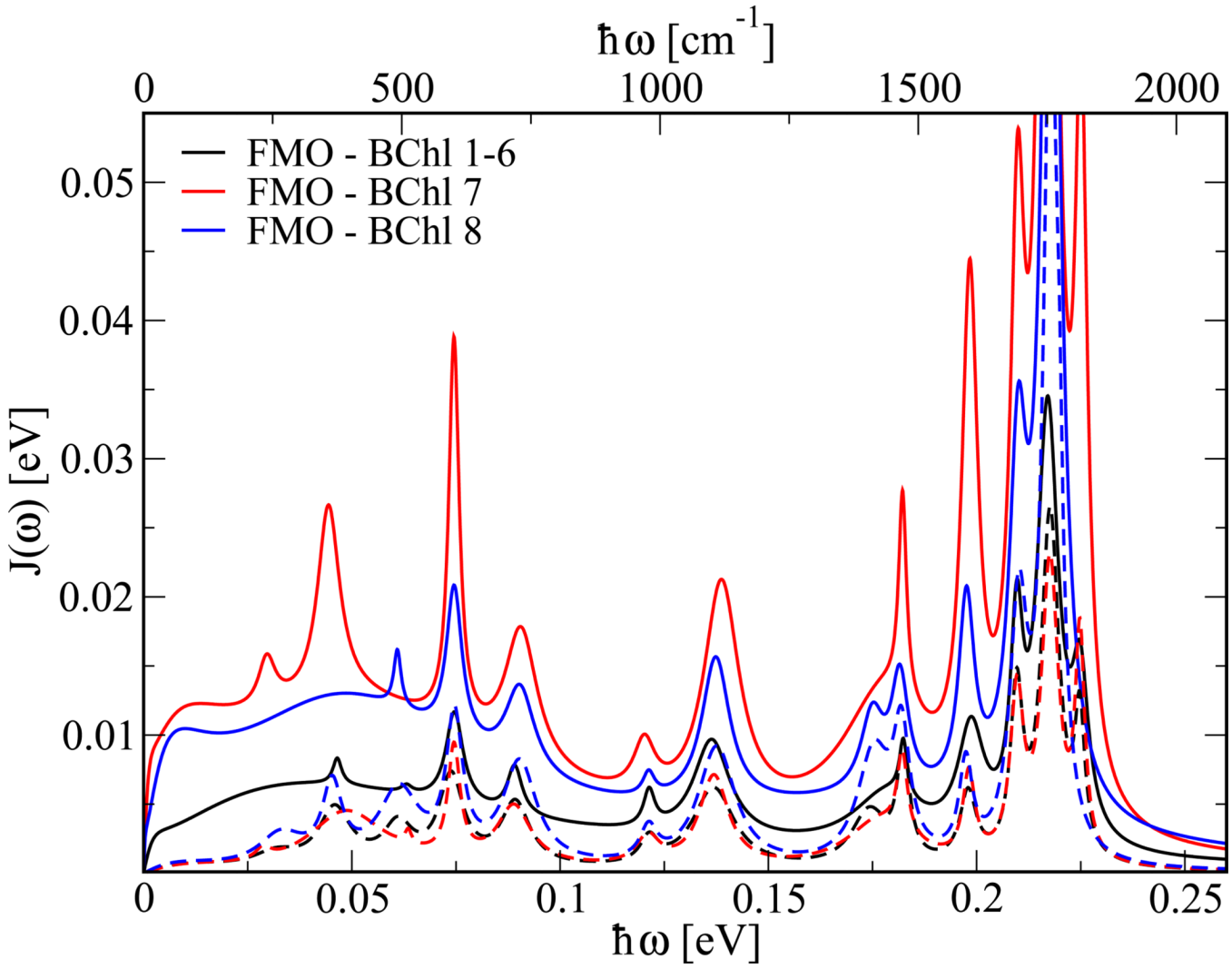

Figure 4.
The solid lines show the same spectral densities as in Fig. 3 while the dashed lines show the spectral densities calculated without taking the external charges into account.

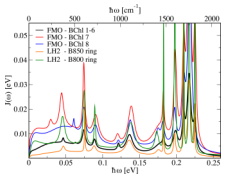

Figure 5.
The spectral densities for the FMO trimer compared to those of the B800 and B850 rings of the LH2 complex.

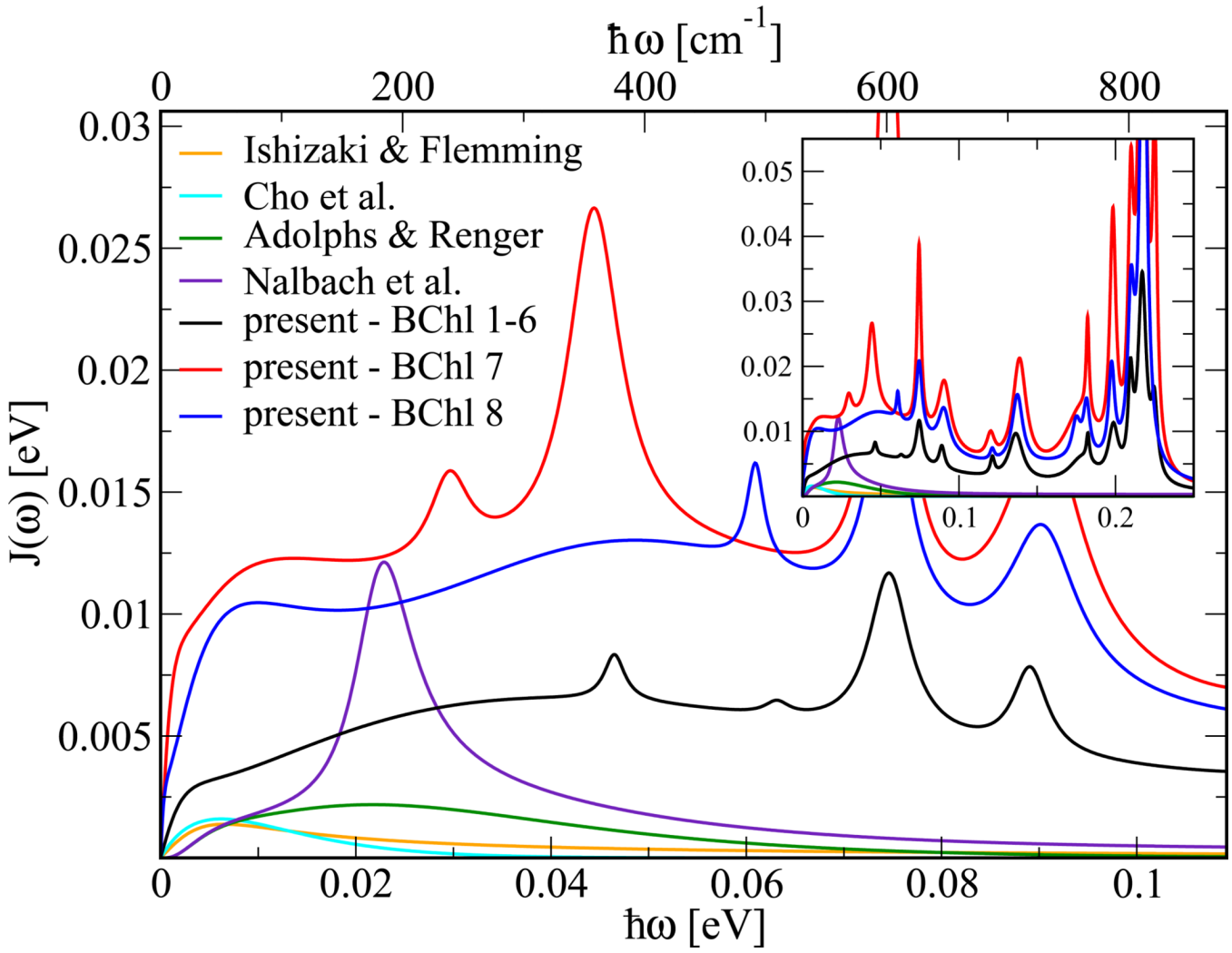

Figure 6.
Spectral densities for the FMO trimer determined in the present study compared to those of previous studies by Ishizaki and Fleming,[11] Cho *et al.*,[34] Adolphs and Renger[33] as well as Nalbach *et al.*[19] The inset shows an enlarged energy and spectral density range.

Table 1

Parameters of Fit 2 for the autocorrelation function based on the trimer simulation data. The correlation functions are averaged over the equivalent pigments in the three monomers. (η_i in [10^{-5} eV^2], $1/\gamma_i$ in [fs])

	BChl 1	BChl 2	BChl 3	BChl 4	BChl 5	BChl 6	BChl 7	BChl 8	BChl 1–6
η_1	275.20	220.55	161.09	233.66	198.44	189.63	525.25	380.18	213.30
$1/\gamma_1$	4.14	4.18	3.99	3.94	4.10	3.79	4.56	4.54	4.04
η_2	80.16	43.03	20.17	46.09	38.64	33.91	146.42	121.77	43.47
$1/\gamma_2$	131.24	166.76	160.87	154.44	118.44	115.79	227.59	140.78	138.98